第13回 X線放射機構(2)

2021年6月15日 5:03

1 . Black body radiation

1. From what kinds of sources will we observe black body emission in X-ray?

熱的な放射 / 光学的に厚いもの → 黒体放射

$$B_\nu(T) = \frac{2}{c^2}\frac{h\nu^3}{e^{h\nu/kT}-1} \ \ [\mathrm{ergs/s/cm^2/Hz/str}]$$

中性子星の表面，白色矮星の表面，活動的な星

ブラックホールや中性子星の周りの光学的に厚い降着円盤

2. Derive the formula of the Planck function for the low-energy limit (Rayleigh-Jeans law) and high-energy limit (Wien function)

$h\nu \ll kT$, $B_\nu(T) \approx \frac{2}{c^2}\frac{h\nu^3}{1+\frac{h\nu}{kT}-1} = \frac{2}{c^2}\frac{h\nu^3}{h\nu}kT = \frac{2}{c^2}\nu^2 kT$

$h\nu \gg kT$, $\frac{2}{c^2}h\nu^3 e^{-h\nu/kT}$

From Rybicki and Lightman

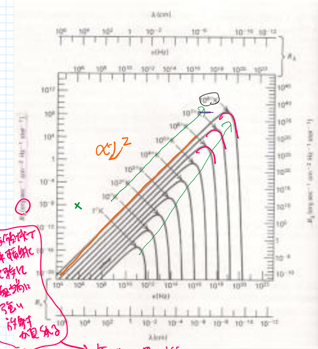

3. Obtain the energy at which the black body energy spectrum (Planck function) peaks.

$E_p \approx 3kT$ ← おぼえる

Use the following formula:
https://www.wolframalpha.com/input/?i=%283+-+x+%29+*+exp%28x%29+%3D+3&lang=en

$$\frac{\partial B_\nu}{\partial \nu} \propto \frac{3\nu^2(e^{\frac{h\nu}{kT}}-1)-\nu^3 e^{\frac{h\nu}{kT}}\cdot\frac{h}{kT}}{(\ \ )^2} = 0$$

$3(e^{\frac{h\nu}{kT}}-1) - e^{\frac{h\nu}{kT}}\cdot\frac{h\nu}{kT} = 0$

$3e^{\frac{h\nu}{kT}} - 3 - e^{\frac{h\nu}{kT}}\cdot\frac{h\nu}{kT} = 0$

$\left(3-\frac{h\nu}{kT}\right)e^{\frac{h\nu}{kT}} = 3$

$\frac{h\nu}{kT} \sim 2.82$

$h\nu = 2.82kT \approx 3kT$

Brightness temperature of 3C273
https://arxiv.org/pdf/1601.05806.pdf

Table 1
RadioAstron ground-to-space radio interferometer measurements of the quasar 3C 273

λ (cm) (1)	Epoch (2)	GRT (3)	r_{uv} (10^3 km; Gλ) (4)	P.A. (deg) (5)	SNR (6)	S_t (Jy) (7)	S_c (mJy) (8)	θ (μas) (9)	T_b (10^{12} K) (10)	$T_{b,min}$ (10^{12} K) (11)	$T_{b,char}$ (10^{12} K) (12)
1.3	2013-02-02	Gb, Y27	103; 7.6	−7	9.8	3.4	125 ± 22	26	14	5.3	12
6.2	2012-12-30	Ar, Ef	90; 1.45	10	18.6	4.3	125 ± 17	142	13	4.5	18
6.2	2013-02-02	Ar	103; 1.69	−8	11.6	4.3	123 ± 19	122	17	5.2	15
18	2013-01-08	Gb	157; 0.87	−32	8.9	5.0	42 ± 7	275	34	4.0	10
18	2013-01-25	Ar, Gb	171; 0.95	−38	12.0	5.0	52 ± 9	246	42	6.3	18

$>10^{13}$ [K]

XSPEC

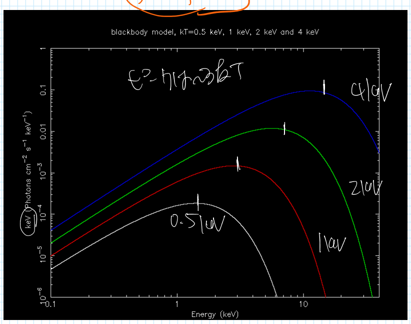

Ebosuzaki 1987, PASJ, 39, 287 X-ray energy spectrum of X-ray burst

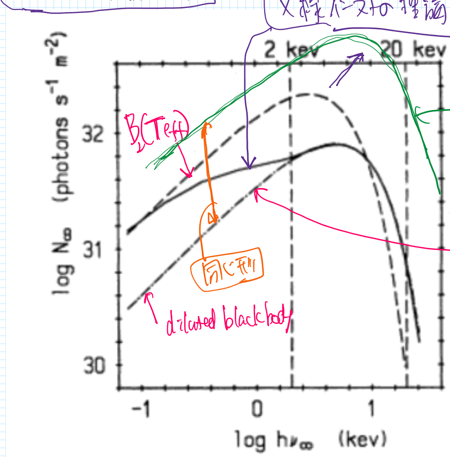

X線バーストの理論計算スペクトル

T_{col} 色温度

$L = 4\pi R^2 \sigma T_{eff}^4$ 有効温度

$T_{col} > T_{eff}$

4. Calculate energy density of the blackbody emission

Use the following formula:
https://ja.wolframalpha.com/input/?i=%E2%88%AB%5B0%2C%E2%88%9E%5D%E5%3F%2F%28exp%28x%29-1%29+dx

$$u = \frac{4\pi}{c}\int_0^\infty B_\nu(T)d\nu \ [\mathrm{erg/cm^3}] = \frac{8\pi}{c^3}\frac{k^4T^4}{h^3}\int_0^\infty \frac{x^3}{e^x-1}dx$$

$$= \frac{8\pi^5 k^4}{15 h^3c^3}T^4 = 7.56\times10^{-15}\,T(\deg)^4\ [\mathrm{erg/cm^3}]$$

5. Estimate the energy density of the 2.7K cosmic microwave background radiation. Compare this with a typical interstellar magnetic energy density with B~3μG.

$7.56\times10^{-15}\cdot(2.7)^4\ [\mathrm{erg/cm^3}] \doteqdot 4\times10^{-13}\ [\mathrm{erg/cm^3}]$

$1\,\mathrm{eV} \approx 1.6\times10^{-12}\,\mathrm{erg}$

$\doteqdot 0.25\ [\mathrm{eV/cm^3}] \sim 0.3\ [\mathrm{eV/cm^3}]$

$\frac{1}{8\pi}(B[\mathrm{Gauss}])^2 = \frac{1}{8\pi}(3\times10^{-6})^2 \sim 0.3\times10^{-12}\ [\mathrm{erg/cm^3}] \approx 0.2\ [\mathrm{eV/cm^3}]$

6. Explain the difference of the effective temperature, color temperature, and brightness temperature

輝度温度　有効温度　色温度 → 黒体輻射 T 同じ

黒体輻射からずれてくる ⇒ 3つが異なってくる。

7. Draw the black body spectrum with the temperature E=kT in a wide energy range using the ν f_ν plot. Observe the energy spectral distribution around kT, if it is widely distributed, or narrowly distributed.
Are there any continuum spectra which are more concentrated (narrowly distributed) around kT?

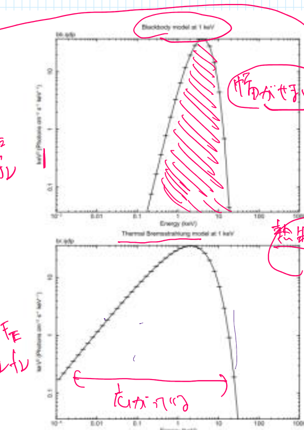

Figure 5.4: Blackbody spectrum with kT = 1 keV (top) and thermal bremsstrahlung spectrum with the same temperature (bottom) in the unite of keV²/s/cm²/keV. Both have peaks at around 3 kT (section 5.3.2). We can see thermal bremsstrahlung is much wide and particularly extends toward lower energies.)

https://arxiv.org/pdf/2003.04962.pdf **XRISM white-paper**

Thermal plasma spectra from clusters of galaxies

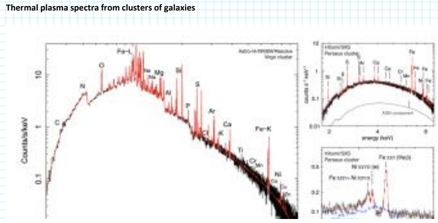

2.Thin-thermal plasma emission

1. From what kinds of sources will we observe thin-thermal X-ray emission?

わせた

ト温度

$B_\nu(T_{cul})\,d\nu$

$^4 \frac{\int B_\nu(T_{cul})\,d\nu}{\sigma T_{cul}^4}$

$4\pi R^2 \sigma T_{eff}^4$

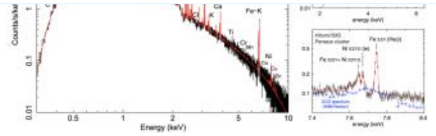

Figure 7: **Left:** *XRISM* simulated spectrum (black) of the core of M87 as observed with 100 ks and the best-fitting model (red). Adapted from[4] **Right:** *Hitomi* spectrum from the core of the Perseus cluster. Broad-band spectrum is shown on the top panel (note that the gate valve was in place during the observation and it absorbs most X-rays below ~ 2 keV), while the zoomed-in on the high-energy end spectrum is shown in the bottom panel. The best-fitting model is shown in red. *Hitomi* resolved individual lines in the spectrum (black vs. blue points)[68].

2. Explain the mechanisms of the continuum emission from thin-thermal plasmas

https://upload.wikimedia.org/wikipedia/commons/1/1e/Bremsstrahlung.svg

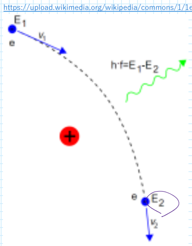

https://www.isas.jaxa.jp/home/ebisawalab/ebisawa/TEACHING/2016Note.pdf

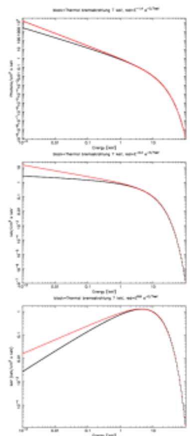

Figure 5.3: Comparison of kT=7 keV thermal bremsstrahlung spectra (black, **bremss** model in xspec) and a cut-off power-law model $\propto E^{-p}\exp(-E/kT)$ where kT=7 keV (red). From top to bottom, unit of the Y-axis is [photon/s/keV/cm^2], [keV/s/keV/cm^2] and [keV^2/s/keV/cm^2], and the p value is 1.4, 0.4, −0.6, respectively.

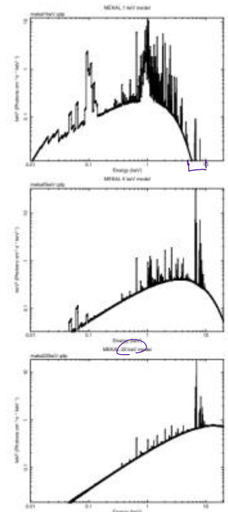

Figure 5.5: Theoretical energy spectra from thermal plasmas at 1 keV, 5 keV and 20 keV. The "mekal" model in XSPEC is used. We can see that, as the temperature increases, (1) the continuum peaks shift toward higher energies, and (2) emission lines from heavier elements are more prominent.

3. If the hot plasma is only composed of hydrogen (protons and electrons), what kind of spectra are expected from thin-thermal plasma?

4. Indicate a simple approximate formula of the thermal bremsstrahlung spectrum.

5. Indicate examples of X-ray energy spectra from thin-thermal plasmas with different temperatures (say, from kT=1 keV to 20 keV). Observe changes of the energy spectra with temperatures paying attention to the following points:
   a. Emission lines
   b. Slope of the continuum in 1 - 10 keV
   c. Peak energy of the continuum

3. Thermal Comptonization

1. Observed how the "cut-off power-law" spectra are formed by thermal (inverse) Comptonization process

2. Observe how the spectral shape changes with the scattering optical depth

3. In which objects the thermal comptonization spectra are expected?

Thermal comptonization model
Pozdnyakov et al. (1983)
http://articles.adsabs.harvard.edu/cgi-bin/get_file?pdfs/ASPRv/0002/1983ASPRv...2..189P.pdf

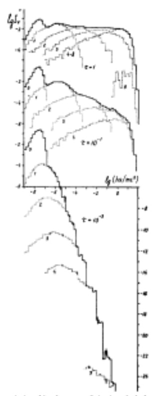

Figure 20 Comptonization of low-frequency radiation in a cloud of weakly relativistic plasma for three values of the optical depth τ. *Dashed curves* represent the contributions of the separate scattering events. The successive scatterings by Maxwellian electrons combine to form a power-law spectrum for the hard radiation.

Longair, "High Energy Astrophysics"

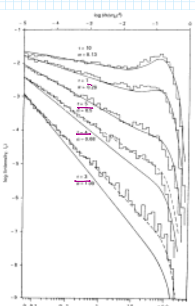

Figure 4.11. The Comptonisation of low frequency photons in a spherical plasma cloud having kT_e = 25 keV. The solid curves are analytic solutions of the Kompaneets equation (see Pozdnyakov *et al.* (1983)); the results of Monte Carlo simulations of the Compton scattering process are shown by the histograms and there is good agreement

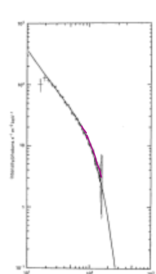

Figure 4.12. The hard X-ray spectrum of the Galactic X-ray source Cygnus X-1 observed in a balloon flight of the Max Planck Institute for Extraterrestrial Physics, on 20 September 1977 compared with the analytic solution of the Kompaneets equation with parameters τ_e = 5, kT_e = 27 keV. (R. A. Sunyaev and L. G. Titarchuk (1980) *Astron. Astrophys.*, **86**, 121.)

https://link.springer.com/content/pdf/10.1007/s00159-007-0006-1.pdf

A widely accepted model for Galactic Black hole binaries

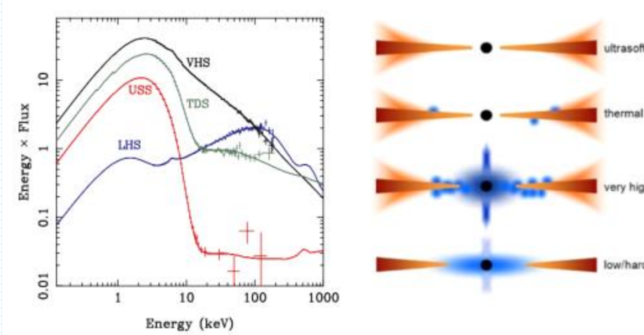

Fig. 9 The *left hand panel* shows a selection of states taken from the 2005 outburst of GRO J
The *right hand panel* shows the proposed accretion flow changes to explain these different spec
differing contributions from the disc, hot inner flow and its associated jet, active regions above the
a wind

AGN accretion geometries under debate
Across the Universe, Research at the Nicolaus Copernicus Astronomical Center, Warsaw 2020

Andrzej A. Zdziarski, Barbara De Marco

Sombreros and lampposts: The geometry of accretion onto black holes

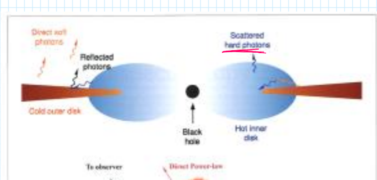

https://ui.adsabs.harvard.edu/abs/1996

Thermal comptonization model for

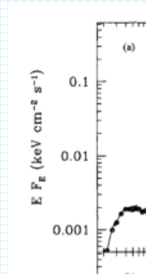

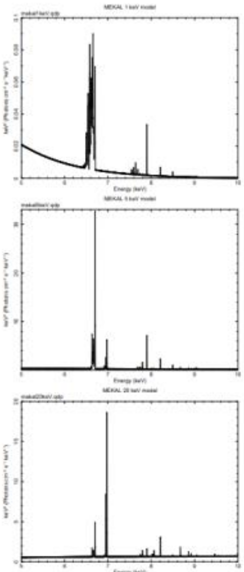

Figure 5.6: Expansion of the iron K-line region in the previous figure. Iron line missions from the 1 keV, 5 keV and 20 keV thermal plasmas are indicated. Around 6.6 – 6.7 keV, FeXXV (He-like) lines are seen, and around 7.0 keV, FeXXVI (H-like) lines are observed. As the plasma temperature increases, lines from more highly ionized ions are observed.

dominant

h

d

1655-40.
tra, with
disc and

MNRAS.283..193Z/abstract

NGC4151

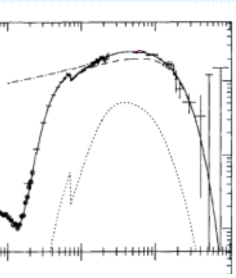

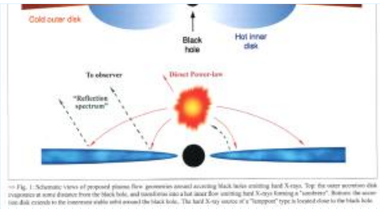

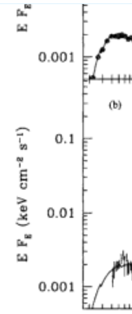

Figure 2. The Xγ spe
June/July by *ROSAT*
ASCA and OSSE. Th
Comptonization spec
ponents, and the sol
spectra. The dot-das
(without the soft X-ra
eters are given in Tab
clarity, and the upper
with circles. The data
added for plotting.

Miyakawa, Ebisawa and Inoue (2012), PASJ,64, 140

Partial Covering Model of MCG –6–30–15

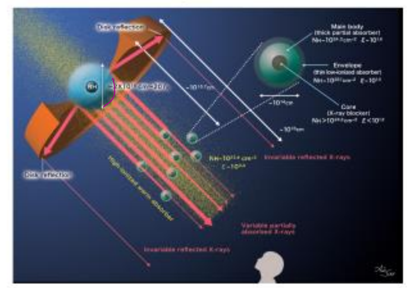

Fig. 12. Schematic picture of the variable partial covering model for MCG –6–30–15 and the internal structure of the absorbing cloud.

4. Non-thermal emission

Often non-thermal **particle acceleration** takes place in the universe (shocks, magnetic acceleration etc.), and each **relativistic** electron ($v \sim c$) has the energy $E = mc^2\gamma$, where $\gamma = 1/\sqrt{1-(v/c)^2} >> 1$

The electron energy distribution N (E) often becomes a power-law, as

$$N(E)dE \propto \gamma^{-p}\, d\gamma.$$

In the case **synchrotron emission** or **relativistic inverse-Compton scattering**, typical photon frequency ν_c from a single electron with the energy $E = mc^2\gamma$ is known to be proportional to γ^2

By integrating over the electron energy distribution, synchrotron spectra or relativistic inverse-Compton spectra may be expressed as

$$F(\nu) \propto \int S(\nu/\nu_c)\gamma^{-p}\, d\gamma.$$

http://cdsads.u-strasbg.fr/pdf/1999MNRAS.309..496G

Thermal compton & non-thermal compton model for Cyg X-1

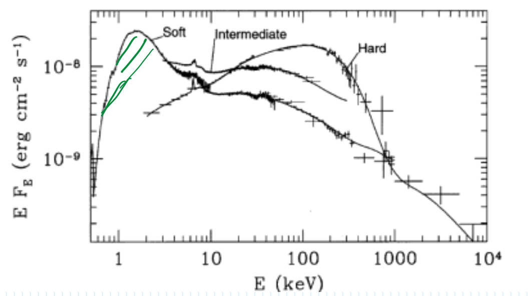

1. Indicate the synchrotron emission or relativistic inverse-Compton scattering spectra become power l-law $\propto \nu^{-s}$

with the index

$$s = \frac{p-1}{2}$$

Synchrotron and Inverse Compton model for the supernova remnant RXJ1713.7-3946

https://www.aanda.org/articles/aa/pdf/2006/13/aa4279-05.pdf

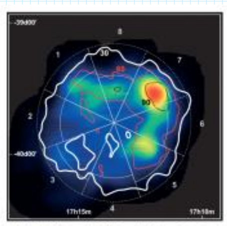

Fig. 15. ASCA X-ray (1–5 keV band, Uchiyama 2005) image of RX J1713.7–3946, overlaid with contours of the smoothed, acceptance-corrected HESS gamma-ray image. The coloured contour levels are labelled and linearly spaced at 30, 60, and 90 counts. Drawn as gray thin lines are eight wedge-shaped regions for which the radial profiles are compared to each other in Fig. 16. Note that in the ASCA image, most of the regions (faint solid lines) do not reach as far as in the HESS image (faint dashed lines), accounting for the limited field of view of ASCA, whose coverage did not always extend to the boundaries of the SNR. As explained in the main text, the ASCA image was smoothed to match the HESS point-spread function to enable comparison of the two images.

http://cdsads.u-strasbg.fr/cgi-bin/nph-iarticle_query?bibcode=1986ApJ...300..522C&db_key=AST&page_ind=12&data_type=GIF&type=SCREEN_VIEW&classic=YES

Synchroton and Inverse-Compton model for Crab pulsar

534 CHENG, HO, AND RUDERMAN Vol. 300

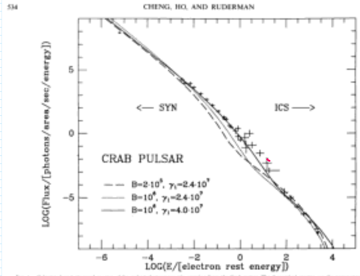

2. Which sources are expected to emit non-thermal comptonization and/or synchrotron emission?

3. When the relativistic electrons, soft input photons (energy density U_{ph}), and magnetic fields (energy density U_B) coexist, both the synchrotron emission and inverse-Comptonization take place simultaneously.
In the case of the SNR RXJ1713.7-3946, observe that the following relationship holds between the synchrotron luminosity (P_{synch}) and the inverse-Comptonization luminosity (P_{compt}).

$$\frac{P_{synch}}{P_{compt}} = \frac{U_B}{U_{ph}}.$$

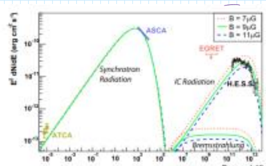

Fig. 19. Broadband SED of RX J1713.7–3946. The ATCA radio data and ASCA X-ray data (Hiraga 2005) for the whole SNR are indicated, along with the HESS measurement and the EGRET upper limit. Note that the radio flux was determined in Lazendic et al. (2004) for the northwest part of the shell only and was scaled up by a factor of two here to account for the whole SNR. The synchrotron and IC spectra were modelled assuming a source distance of 1 kpc, an age T of 1000 years, a density n of 1 cm^{-3}, and a production rate of relativistic electrons by the acceleration mechanism in the form of a power law of index $\alpha = 2$ and an exponential cutoff of $E_0 = 100$ TeV. Shown are three curves for three values of the mean magnetic field: 7 μG, 9 μG, and 11 μG, to demonstrate the required range of the B field strength for this scenario. The electron luminosity is adopted such that the observed X-ray flux level is well matched. For the three magnetic field values the luminosity L_e is $L_e = 1.77 \times 10^{37}$ erg s^{-1} (7 μG), $L_e = 1.14 \times 10^{37}$ erg s^{-1} (9 μG), and $L_e = 0.81 \times 10^{37}$ erg s^{-1} (11 μG).

4. In Fig. 19 of Aharonian et al. 2006, the relativistic electron energy distribution has been assumed to be $\gamma^{-p} \exp(-mc^2\gamma/E_c)$, where p is 2 and E_c=100 TeV.

Explain the following values semi-quantatively:
(a) Inverse Compton spectral peak energy
(b) Cut-off energy of the synchrotron spectrum and the inverse Compton spectrum
(c) Slope of the synchrotron spectrum and the inverse Compton spectrum below the cut-off energies

https://iopscience.iop.org/article/10.1088/0004-637X/773/2/138/pdf

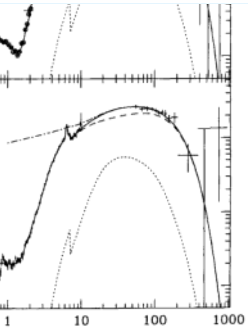

ectra of NGC 4151 as observed (a) in 1991
, *Ginga* and OSSE, and (b) in 1993 May by
he dashed curves give the absorbed thermal
tra, the dotted curves give the reflection com-
id curves give the models of the observed
shed curves give the unabsorbed continua
y excess and the Kα line). The model param-
le 1. The plotted data have been rebinned for
limits are 2σ. The *ROSAT* data are marked
from all four *ASCA* detectors have been co-

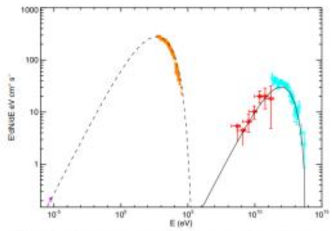

Figure 3. Spectral fit to observations of SNR RX J1713.7-3946 with a 2D MHD simulation. The different emission processes are synchrotron (dashed line), IC (solid line). The data are from Acero et al. (2009; in radio), Tanaka et al (2008; *Suzaku* X-ray), Abdo et al. (2011; *Fermi*-LAT), and Aharonian et al. (2006; HESS). Note that the two lowest energy *Fermi*-LAT points are upper limits. The seed photon field in the IC process includes an IR component with a temperature of $T = 30$ K and an energy density of 1.2 eV cm^{-3} and the microwave background radiation (Li et al. 2011).